



**EUROfusion**

WPMST1-CPR(17) 17254

ME Maraschek et al.

**Path-oriented early reaction to  
disruptions in ASDEX Upgrade and TCV  
in view of the future needs for ITER and  
DEMO**

Preprint of Paper to be submitted for publication in Proceeding of  
44th European Physical Society Conference on Plasma Physics  
(EPS)



This work has been carried out within the framework of the EUROfusion Consortium and has received funding from the Euratom research and training programme 2014-2018 under grant agreement No 633053. The views and opinions expressed herein do not necessarily reflect those of the European Commission.

This document is intended for publication in the open literature. It is made available on the clear understanding that it may not be further circulated and extracts or references may not be published prior to publication of the original when applicable, or without the consent of the Publications Officer, EUROfusion Programme Management Unit, Culham Science Centre, Abingdon, Oxon, OX14 3DB, UK or e-mail [Publications.Officer@euro-fusion.org](mailto:Publications.Officer@euro-fusion.org)

Enquiries about Copyright and reproduction should be addressed to the Publications Officer, EUROfusion Programme Management Unit, Culham Science Centre, Abingdon, Oxon, OX14 3DB, UK or e-mail [Publications.Officer@euro-fusion.org](mailto:Publications.Officer@euro-fusion.org)

The contents of this preprint and all other EUROfusion Preprints, Reports and Conference Papers are available to view online free at <http://www.euro-fusionscipub.org>. This site has full search facilities and e-mail alert options. In the JET specific papers the diagrams contained within the PDFs on this site are hyperlinked

# Path-oriented early reaction to approaching disruptions in ASDEX Upgrade and TCV in view of the future needs for ITER and DEMO

M.Maraschek<sup>1</sup>, A.Gude<sup>1</sup>, V.Igochine<sup>1</sup>, H.Zohm<sup>1</sup>,  
E.Alessi<sup>3</sup>, M.Bernert<sup>1</sup>, C.Cianfarani<sup>4</sup>, S.Coda<sup>2</sup>, B.Duval<sup>2</sup>, B.Esposito<sup>4</sup>, S.Fietz<sup>1</sup>, M.Fontana<sup>2</sup>,  
C.Galperti<sup>2</sup>, L.Giannone<sup>1</sup>, T.Goodman<sup>2</sup>, G.Granucci<sup>3</sup>, L.Marelli<sup>5</sup>, S.Novak<sup>3</sup>, R.Paccagnella<sup>5</sup>,  
G.Pautasso<sup>1</sup>, P.Piovesan<sup>5</sup>, L.Porte<sup>2</sup>, S.Potzel<sup>1</sup>, C.Rapson<sup>1</sup>, M.Reich<sup>1</sup>, O.Sauter<sup>2</sup>, C.Sozzi<sup>3</sup>,  
G.Spizzo<sup>5</sup>, J.Stober<sup>1</sup>, P.Zanca<sup>5</sup>, ASDEX Upgrade team, TCV team, the EUROfusion MST1 Team<sup>6</sup>

<sup>1</sup> Max-Planck-Institut for Plasmaphysics, D-85748 Garching, Germany

<sup>2</sup> Ecole Polytechnique Fédérale de Lausanne (EPFL), Swiss Plasma Center (SPC), 1015, Switzerland

<sup>3</sup> IFP-CNR, via R. Cozzi 53, 20125 Milano, Italy

<sup>4</sup> ENEA, Fusion and Nuclear Safety Department, C. R. Frascati, 00044 Frascati (Roma), Italy

<sup>5</sup> Consorzio RFX, corso Stati Uniti 4, 35127 Padova, Italy

<sup>6</sup> see the author list in [H. Meyer et al., Nuclear Fusion FEC 2016 Special Issue (2017)]

E-mail: Maraschek@ipp.mpg.de

PACS number: 52.55.Fa, 52.55.Tn, 28.52.Cx, 28.52.Cx

Keywords: tokamak, disruption avoidance, sensor, actuator, control

**Abstract.** Routine reaction to approaching disruptions in tokamaks is currently restricted to machine protection, which obviously remains a basic requirement for ITER and DEMO. However, in future fusion devices, high performance discharge time itself will be very valuable. The ultimate goal is therefore to actively avoid approaching disruptions and sustain the discharges whenever possible. To achieve this, the knowledge of the most relevant possible root causes and the corresponding chain of events leading to disruption, the disruption path, is vital. For each disruption path, physics-based sensors and adequate actuators must be defined and their limitations considered. Early reaction facilitates the efficiency of the actuators and enhances the probability of a full recovery. Thus, sensors that detect potential disruptions in time are to be identified.

The hierarchy of action should be (I) recovery of the discharge to full performance or at least continuation with a less disruption-prone backup scenario, (II) complete avoidance of the disruption to sustain the discharge or at least delay it for a controlled termination and, (III), only as worst choice, a disruption mitigation. Based on the understanding about disruption paths, a hierarchical and path-specific handling strategy must be developed. Such schemes, tested in present devices, could serve as a blueprint for ITER and DEMO operation.

For some disruption paths, experiments have been performed at ASDEX Upgrade and TCV. Disruptions were provoked in ASDEX Upgrade by reaching the density limit both in L and H-modes and in TCV by impurity injection into ELMy H-mode discharges. The new approach described in this paper has been partially implemented for the H-mode density limit and the impurity injection experiments. Sensors used so far react too late for the H-mode density limit. A state-space boundary is proposed, that can serve as an adequate sensor for avoiding density limit disruptions from H-mode scenarios.

## 1. Introduction

Disruptions are a major concern for any tokamak as both the wall heat load by the thermal energy quench, as well as the electromagnetic forces generated during the current quench can cause problems. Present experiments mainly focus on reducing these thermal and mechanical loads by mitigating the disruption. At present, this involves the injection of large amounts of radiating impurities that quickly reduce the plasma energy and raise the density in order

to avoid the formation of electron runaway beams. These discharges still disrupt and cause thermal and mechanical loads. However, the implementation of the required fast gas injection valves in the harsh environment of ITER is more difficult than originally anticipated [1].

In future devices, such as ITER and DEMO, disruption mitigation must therefore be restricted to the absolutely unavoidable cases. Additionally, discharge time is valuable, such that a premature termination of a running discharge even by a controlled

ramp down has to be avoided, provided a continuation is possible without risking a damage. With these more demanding requirements compared to presently implemented control schemes, the discharge control and the handling of near disruption states should be reconsidered. This modified approach ultimately should provide the basis for the operation of ITER and DEMO.

The paper is structured as follows. In section 2, the present status of dedicated experiments and the routine handling of disruption is briefly summarized. In section 3, a new generalized approach on disruption handling is proposed. In section 4 and 5, the latest experiments at ASDEX Upgrade and TCV are described. Finally, in section 6, the present results and some discussion about the new considerations are summarized.

## 2. Disruption handling in present tokamaks

### 2.1. Paths leading to disruptions

To better understand and handle disruptions, the root causes of disruptions were analyzed for JET with its original carbon wall [2]. Later, analysis of the ITER-like wall (tungsten and beryllium) at JET [3] and of ASDEX Upgrade (AUG) with its tungsten wall [4] was performed. Based on these classifications the most important types of disruptions and their causes were extracted (see table 1). Each type of disruption is following a natural sequence of events, its path  $path_i$ , until the discharge disrupts. Such paths may be used as the physics basis for disruption handling in upcoming experiments. For each path a stability limit is reached. In the following we briefly describe these paths.

root cause	description
Vertical Displacement Event (VDE)	fast vertical displacement due to loss of control
L-mode $n_e$ limit	edge limit, MARFE, $T_e$ and $I_p$ peaking, n=1 modes
H-mode $n_e$ limit	edge limit, HL-transition, MARFE, late n=1 modes
$\beta_N$ limit	pressure driven resistive or ideal core MHD, mode locking
high-Z impurity accumulation	metal wall issue, radiation peaking and losses, resistive MHD mode in the core
technical failure	irregular influx or drop of material or debris, control system failure, power supply failure, ...

**Table 1.** List of most important disruption types identified from AUG and JET.

The vertical displacement event (VDE) is the strongest positional instability and can be very fast. This is typically a loss of the vertical stability of the plasma, which no longer can be handled by the control system using shaping and position control coils. The velocity of the displacement is governed by the time constants of the induced mirror currents in the vessel. In present experiments such events remain unavoidable. A mitigation of the resulting disruption is the only viable control reaction [5].

In the density limit (DL), both in L-mode and in H-mode, the plasma is strongly cooled from the edge by a too high particle influx. In both cases an X-point radiator is formed, which was named MARFE (Multi-faceted Assymetric Radiation From the Edge) [6] in experiments with carbon wall and was less stable compared to the present situation with metallic walls. The edge cooling leads to central peaking of the temperature and hence the current profile, increasing the likelihood of MHD activity. Typically tearing modes with toroidal mode number  $n = 1$  are initiated and, once toroidally coupled with different poloidal mode numbers,  $m$ , over multiple resonant surfaces, lead to a disruption. These modes are thus not the disruption root cause, but a result of the discharge development. In the H-mode DL edge cooling first leads to an H to L-transition and finally to DL disruption in L-mode [7, 8, 9]. In [9] the HL-transition is described in terms of the stored energy  $W_{mhd}$  and a line integrated edge density measurement ( $\rho_p \geq 0.7..0.8$ ). This approach plays a central role in developing a state-space based sensor of the H-mode density limit (section 4).

In the ideal or resistive high  $\beta_N$  limit, the pressure and hence its gradient at resonant surfaces increase to a value where resistive or ideal MHD limits are reached and a possible disruptive MHD mode can be triggered. This is typically the Neoclassically driven Tearing Mode (NTM), which is caused by a loss of bootstrap current within the islands O-point. Depending on the discharge scenario, faster growing ideal modes can also be triggered at higher  $\beta_N$ .

In experiments with metallic walls (for example AUG with its tungsten wall or JET with an ITER-like wall with a combination of tungsten and beryllium), high-Z impurities can enter the plasma. Owing to neoclassical transport, they accumulate in the plasma centre and act there as a strong radiator as they are not fully ionized. This core radiation cools the plasma and generates hollow temperature profiles. This makes the discharge unstable and initiates the disruption [10, 11].

Additional to these operational limits on plasma stability, technical failures may occur. These events are typically mechanical failures leading to a release of impurities or debris falling into the vacuum chamber.

Depending on the severity of the failure, this can produce various chains of events that lead to a disruption. Externally, the control system or the power supply of an experiment may fail and measures have to be foreseen, to handle such events. Finally, actuator failure (such as NBI or ECRH power loss) can cause disruptions that depend on the specific control and plasma conditions.

## 2.2. Sensors

A dedicated set of measurements is required to handle an approaching disruption and identify the proximity to an operational boundary for a specific disruption  $path_i$ . This must be obtained well in advance to control the appropriate handling for that  $path_i$ . These sensors must be always available during the discharge in real-time and reliably detect the relevant plasma parameters for the considered disruption type. Such sensors are not necessarily simple scalar measurements, but might be complex combinations of signals describing the plasma state in a generic state-space. Table 2 gives an indication of such sensors which fulfil these conditions with increasing complexity.

sensor	action		
VDE detector			III
loop voltage rise		II	III
locked mode detector		(II)	III
$n = 1, n = 2$ mode detector	(I)	II	
entropy $H$ from rt-SVD	I	(II)	
$n_e$ and radiation peaking (interferometer, bolometer, soft X-ray)	I	(II)	
MARFE detectors (bolometer, bremsstrahlung, detachment via $H_\alpha$ in the divertor)	I	II	
state space observer (such as RAPTOR)	I	II	III
state space predictor ("flight simulator")	I	II	III

**Table 2.** List of sensors and for which type of action they are mostly relevant (see section 3.1.)

The vertical displacement detector is generated by a real-time comparison between the requested plasma z-position and the z-position from the real-time equilibrium reconstruction. As avoidance as no longer feasible for a deviation larger than a given threshold, this triggers an immediate mitigation reaction at AUG.

Typically, an existing perturbation in the plasma, such as a large MHD mode, increasing radiation losses or current profile peaking, leads to an increase of the loop voltage,  $U_{loop}$ , to maintain the requested

plasma current,  $I_p$ . Either a pre-defined threshold or a discharge condition dependent dynamical threshold on  $U_{loop}$  serves as a trigger for reactions of the control system.

One common feature in the later phases of disruptions are locked modes (LM). In principle they can be detected easily by a linear combination of at least 4 toroidally distributed saddle coils to obtain the field amplitude,  $B_r^{pert}$ , and its phase [12]. LMs typically occur only very shortly before the disruption and are mainly useful for triggering mitigation actions.

Various detection schemes exist for MHD modes during their early phase while they are still rotating. To identify the potential threat of specific modes, an identification of the toroidal and poloidal mode numbers,  $n$  and  $m$ , is required. The mode numbers obtained through the analysis of a spatially distributed set of Mirnov coils, that measure the perturbation field  $B_\theta^{pert}$  or  $B_r^{pert}$ . Techniques that employ individual coils only do also exist [13], but rely upon specific assumptions. Recently, a newly established method that uses a real-time singular value decomposition (SVD) analysis was implemented at FTU, and ported to AUG and TCV [14]. The SVD calculates the correlation of the Mirnov coil signals, which typically increases long before the amplitude of the corresponding perturbation field raises over a reliably detectable threshold. This is implemented via the calculation of the entropy  $H$  from the eigenvalue distribution of the SVD [14], which is a measure of degree of correlation in the original signal. It also provides likelihoods for multiple  $m, n$  combinations, and allows the mode identification. The use of real-time correlation analysis of the magnetics together with measurements of the local electron temperature (ECE), provides the radial localization and the eigenfunction of the modes [15].

In the high-Z impurity induced  $path$  the increase together with the peaking of the core plasma radiation is a clear indicator for the disruption proximity. This is typically calculated from several lines of sight of a bolometry system. SXR emissivity is useful, but suffers from the combined dependence of the emission on the impurity concentration, the impurity type and local temperatures. A summary on the behaviour of disruptions with metallic walls has been given in [11].

The MARFE, or X-point radiator can be detected through a tomographic inversion of a bolometer array. With increasing computing power, such calculations are able to detect the MARFE formation together with its radial and vertical location [16]. In older experiments also the divertor detachment, detected from the  $H_\alpha$  emission of the inner and outer divertor, has been used as a measure of the detachment degree and hence the operational proximity of a MARFE

formation in AUG. The MARFE itself was detected from the X-point emission of bremsstrahlung [17].

The combination of multiple signals allows the definition of a plasma state within a state space observer. Such states are able to characterize the proximity to operational boundaries of the plasma and then used to initiate avoidance measures. In this framework a real-time density observer has been implemented at AUG to provide density profile information [18, 19] (see section 4).

### 2.3. Actuators and dedicated experiments

Once an approaching disruption has been detected with physics based disruption identifiers, a set of possible actuators are available to mitigate or avoid disruptions in the specific scenario. Table 3 lists an overview of such actuators.

actuator	action
central wave heating: ECRH, ICRH	I II
local heating/current drive: ECRH/ECCD	I II (III)
increase of $P_{heat}$	I II
RMPs for error field compensation	I II
RMPs for mode entrainment	II
RMPs + ECCD/ECRH	II (III)
massive gas injection (MGI), killer pellet, shattered pellets (highest amount of injected mass)	III III III

**Table 3.** List of actuators and for which type of action they are mostly relevant (see section 3.1.)

For high Z impurity accumulation in devices with metal walls, the most important actuator is central heating without additional central particle fuelling. At AUG and JET this is achieved by central wave heating ( $\rho_p \approx 0$  within the  $q=1$  surface) with ECRH or ICRH [20]. This application routinely stabilizes discharges on both experiments and will be a prerequisite for the operation of ITER. However, already in ITER the central heating will be largely dominated by the  $\alpha$ -particles, which non-linearly depends on the plasma conditions. It is not yet clear whether the external heating will be able to replace a loss of the  $\alpha$ -heating.

In scenarios where ideal or resistive MHD play the dominant role for the disruption (i.e. in the high  $\beta_N$ -limit) local ECCD current drive at the resonant surface of the MHD is the most appropriate tool. This falls into the topic of NTM stabilization of the (2/1)-mode that has been performed on various experiments [21, 22, 23, 24]. The additional combination with external resonant magnetic perturbations (RMP) allows the control of the island phase and to steer the, now

modulated, ECCD only into the island's O-point [25, 26, 27]. The RMPs can also be used to avoid the locking of an MHD and entrain the mode to keep it rotating. However, effective RMP application requires a low enough density and high enough  $\beta$ . Low density is required for the perturbation field to penetrate up to the resonant surface and high  $\beta_N$  is needed to take advantage of resonant field amplification [28].

Both in the L-mode and H-mode density limit  $n = 1$  modes occur that play a central role in the final thermal and current quench. These modes can be addressed in the same way as NTMs by local heating or current drive at the resonant surface. The local change of the current profile, either by external current drive or the modification of the conductivity via the local temperature rise stabilizes the mode. This can be seen as a modification of the local stability parameter,  $\Delta'$ , from the classical Rutherford equation.

Recent L-mode experiments were able to further increase the density nearly a factor of 2 above the limit at which the disruption set in [29]. One central gyrotron for heating and one gyrotron for current drive at the  $q=2$  surface were used. Attempts to adapt this scheme for the H-mode density limit with the application of ECCD will be discussed in section 4.

Alternatively, increasing radiation losses with increasing density can be counteracted with increased heating power. This was successfully and routinely done with additional NBI heating on AUG, which was triggered by the divertor detachment sensor [17], and with additional central ICRH, as it has been demonstrated on ADITYA [30]. At AUG, the use of additional NBI heating power and a control of the applied gas influx was used routinely with the carbon wall to avoid density limit disruptions. However, such ideas will again have to compete with the loss of  $\alpha$ -particle heating in future devices.

For disruption mitigation, the deliberate massive density increase is employed in order to radiate as much energy as possible, for cases where a disruption is considered inevitable. A massive increase in density also suppresses a possible electron runaway current [31]. This mitigation is used routinely for machine protection by a dedicated massive gas injection (MGI) [32]. Injection of killer pellets with impurities has been tested [33, 34]. Recently, shattered pellet injection, which is foreseen for ITER [1], has been established in DIII-D [35].

Along these described lines, most of the attempts to avoid disruptions must still be considered as proof of principle experiments for the specific scenario. A combination of the sensors and actuators in an automatic protection scheme has yet to be implemented but is urgently required for future experiments. The next section describes the approaches that are presently op-

erational.

#### 2.4. Present routine disruption handling

On present devices, only a very limited number of sensors and actuators are used routinely. At AUG, the locked mode detector triggers either an early soft plasma discharge ramp down or an MGI, (for  $I_p > 0.85\text{MA}$ ) for disruption mitigation, depending on the mode size. For a VDE, the MGI is triggered instantaneously. Following some technical failures of the control system or the power supplies, the MGI is also initiated. However, the MGI always injects a large but fixed amount of gas independent of the discharge evolution.

At JET, the LM and the  $n=1$  or  $n=2$  amplitudes also trigger a soft discharge ramp down. Often this leads to unavoidable and unmitigated disruptions during the  $I_p$  ramp down. An automatic MGI trigger from the LM detector has become a necessity for the operation with the ITER like wall [11].

No present day experiment has implemented a routine branching to a backup program. Similarly, no experiment has implemented an automatized disruption reaction for avoidance or mitigation.

### 3. Generalized approach

All the above indicated concepts for identifying disruption categories and connecting them to their  $path_i$  (such as  $\beta_N$ -limit,  $path_{\beta_N}$ , the L-mode density limit,  $path_{LDL}$ , or the H-mode density limit,  $path_{HDL}$ ) have to be combined into a complete framework.

#### 3.1. Categorization of actions

The action which has to be applied to the plasma will necessarily be situation dependent. It will not only depend on the  $path_i$  on which the discharge develops. The required action will also have to take into account the severity of the situation. We suggest the following principal type of actions, which have to be defined for each  $path_i$ .

- **I: recovery** of the discharge to its full original performance, by moving it away from the operational boundary
- **II: avoidance** of the disruption when the discharge is already very close to an operation boundary
- **III: mitigation** of the ongoing disruption, if inevitable

In present dedicated experiments the disruption path is pre-selected by the type of discharge which is performed. For each experiment, the sensors,  $\Sigma_j sensor_{i,j}$ , are individually selected. For the action,

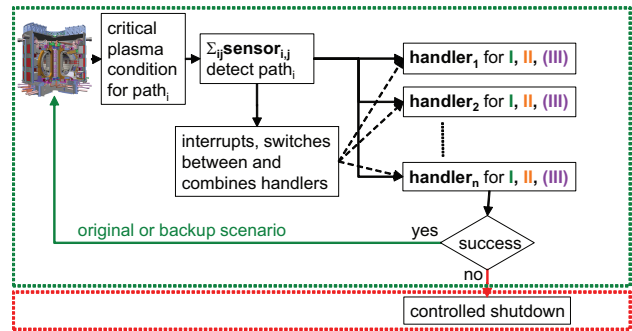


**Figure 1.** Flow diagram of the outer control loop, which has to detect, which  $path_i$  towards a disruption has the highest probability and activates the corresponding  $handler_i$  (figure 2). This controller needs to have the ability to interrupt, exchange or combine handlers, if another path causes a larger threat during the activity of a handler. The green area is the desired operational area, whereas the red area, an unwanted controlled shutdown, should be avoided.

$action_{i,k}$ ,  $k = \text{I:recovery, II, avoidance, III, mitigation}$ , a set of actuators,  $\Sigma_{k,m} actuator_{i,k,m}$ , can be used. Note that both sensors and actuators might be needed for multiple paths and an actuator management might be needed.

#### 3.2. Flow diagrams for the disruption handling

Our approach can be easily understood with the help of flow diagrams. The outer part of the controller (figure 1) has the task of identifying the proximity to a specific disruption  $path_i$  by using all available sensors and state space information. Once a  $path_i$  is identified, the corresponding handler,  $handler_i$  (figure 2), is activated. If during the activity of this  $handler_i$  another  $path_j, j \neq i$  becomes a larger threat, the supervisor must be able to interrupt the  $handler_i$  and switch to  $handler_j$  or combine their activity with possibly shared use of sensors and actuators.

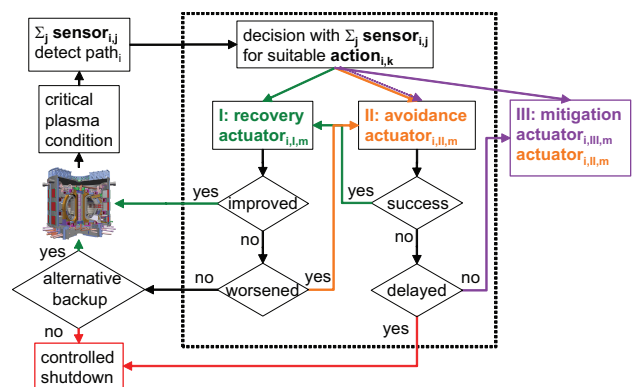


**Figure 2.** Flow diagram of the  $handler_i$ , which has to be defined for each disruption  $path_i$  individually. The dotted rectangle defines the handler boundary. The handler applies the actuators for its 3 possible actions. The mitigation action (III) should be implemented again externally.

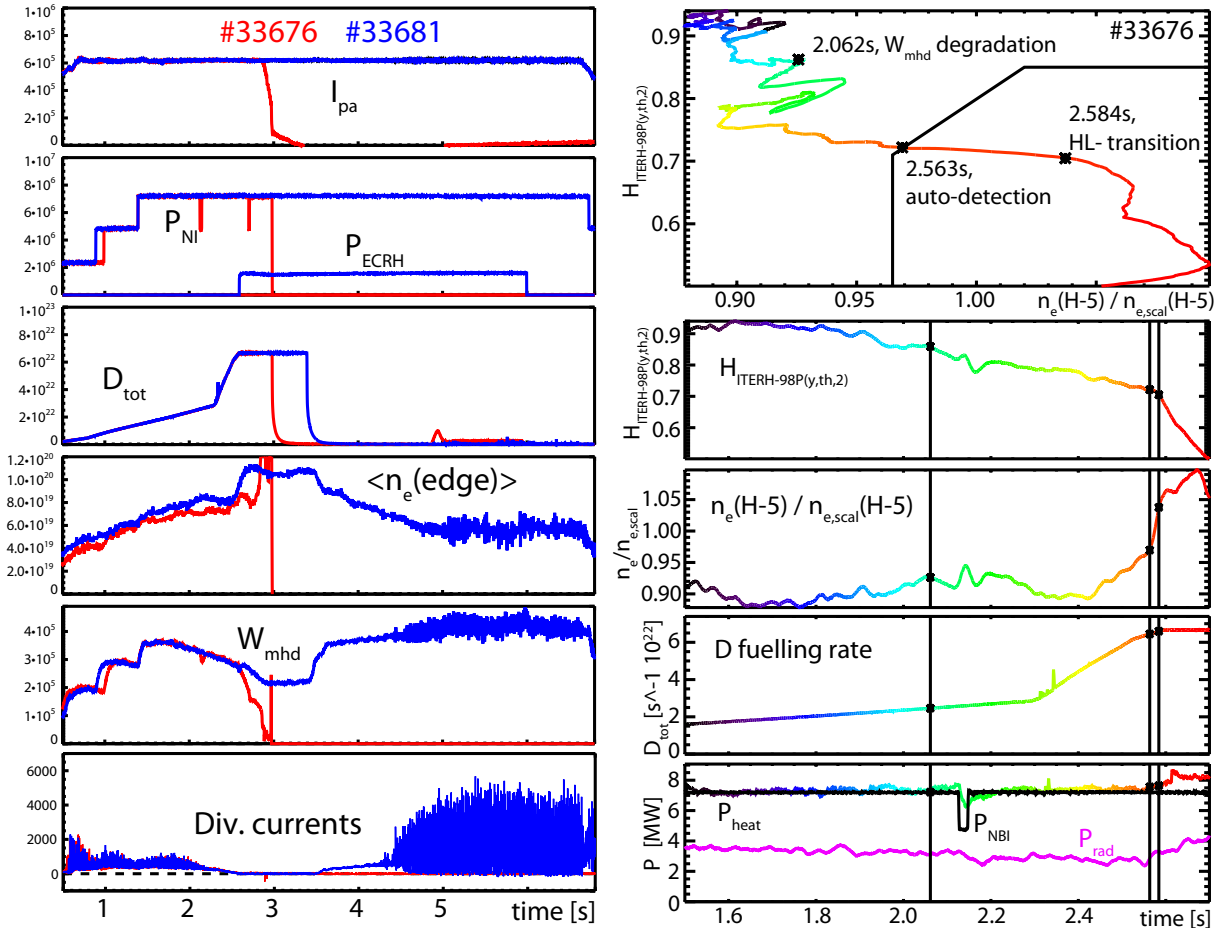


**Figure 3.** Left figure: Time traces of a disrupting reference density limit discharge #33676 and discharge #33681, where the disruption could be avoided with the application off ECCD and the confinement could be recovered by removing the strong gas puff. The traces show the plasma current  $I_{pa}$ , the NBI heating power  $P_{NBI}$  and the applied ECCD  $P_{ECRH}$ , the feedforward gas puff rate  $D_{tot}$ , the stored energy  $W_{mhd}$  and the outer divertor currents. Right figure: For the disrupting discharge the trajectory in terms of  $n_e(H-5)/n_{e,scal}(H-5) - H_{ITERH-98P}(y,th,2)$  is shown. The time is coded in rainbow colours. For orientation below the traces of  $H_{ITERH-98P}(y,th,2)$ ,  $n_e(H-5)/n_{e,scal}(H-5)$ ,  $D_{tot}$ ,  $P_{tot}$ ,  $P_{NBI}$  and total radiated power  $P_{rad}$  as function of time are shown.

The path specific sensors,  $\sum_j sensor_{i,j}$ , within the handler support the decision about which of the recovery, avoidance or mitigation actions need to be taken. The  $handler_i$  uses the available  $actuators_{i,k,m}$  in its  $path_i$  to achieve its mission of regaining safe plasma operation. At every time step, the judgment between the actions must be repeated. If safe operation can be achieved it gives control back to the outer part, or initiates a controlled shutdown if not possible. Apart from possible technical failures, mitigation should not be needed and the discharge should continue.

The MHD controller at ASDEX Upgrade has implemented such a control scheme with prioritization of the required actions and appropriate actuator management for the application of central ECRH for avoiding impurity and radiation peaking, the removal of still rotating (2/1)-NTMs and (3/2)-NTMs [36, 37, 38]. The MHD controller has managed, depending on the occurrence of radiation peaking, (3/2) or (2/1)-

NTM's, the radial location where the ECRH/ECCD has to deposit its power. This does not yet include the disruption considerations. This can serve as a blueprint for the further implementation of the presented ideas. Similar approaches are performed at TCV [39].

### 3.3. Steps for the implementation

In order to implement the proposed scheme the following list of actions should be executed.

- 1: create or use statistical data analysis for the most likely root cause of disruptions and describe the  $path_i$  leading to the disruption
- 2: identify appropriate sensors,  $sensor_{i,j}$  for that  $path_i$
- 3: identify appropriate actuators for the recovery (I), avoidance (II) and mitigation (III) of this path, i.e.  $actuator_{i,I,k}$ ,  $actuator_{i,II,k}$  and  $actuator_{i,III,k}$

- 4: implement the specific handler,  $handler_i$  for that path, which uses these actuators and sensors
- 5: repeat step 2-4 for all identified paths from 1
- 6: create a supervisor managing the handlers

#### 4. H-mode density limit on ASDEX Upgrade

The H-mode density limit is a two step process. At sufficiently high density,  $n_e$ , the H-mode confinement degrades typically with type III ELMs. If  $n_e$  increases further, the discharge transits to an L-mode. In L-mode, the discharge disrupts usually with current profile peaking and  $n = 1$  tearing modes. Depending on  $q_{95}$ , either a (2/1) or (3/1) tearing mode is the dominant actor. In [9], a scaling for this H to L-transition at AUG is given in terms of the line integrated density  $\bar{n}_e$  of a peripheral line of sight of the DCN interferometer (channel H-5, with  $\rho_p \geq 0.7 \dots 0.8$ )

$$\bar{n}_{e,scal}(H-5) = (0.506 \pm 0.192) \frac{P_{heat}^{0.396 \pm 0.13} I_p^{0.265 \pm 0.14}}{q_{95}^{0.323 \pm 0.14}}, \quad (1)$$

where  $I_p$  is in MA,  $P_{heat}$  in MW and  $\bar{n}_{e,scal}$  in  $10^{20} m^{-2}$ . For this scaling, a very slow gas puff ramp or a constant gas puff rate was used. A wide range of heating power ( $6 MW \leq P_{heat} \leq 12.5 MW$ ), safety factor ( $3.5 \leq q_{95} \leq 6$ ), plasma current ( $0.6 MA \leq I_p \leq 1.2 MA$ ), toroidal magnetic field ( $1.45 T \leq B_t \leq 2.7 T$ ) and triangularity ( $0.23 \leq \delta \leq 0.37$ ) was employed.

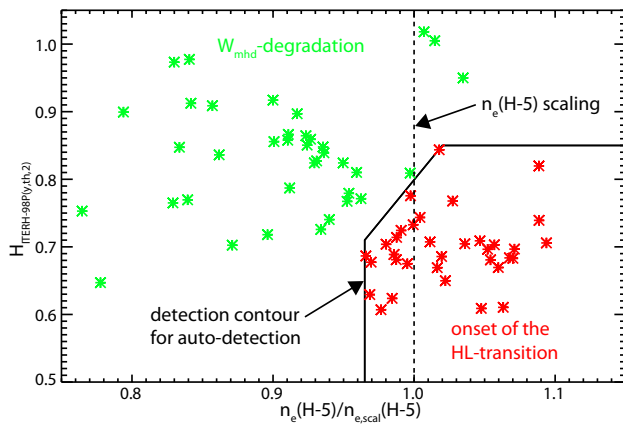


**Figure 4.** Operation diagram in terms of  $n_e(H-5)/n_{e,scal}(H-5)$  versus  $H_{ITERH-98P(y,th,2)}$ . The light green points represent the times when the discharge performance already degrades in terms of  $H_{ITERH-98P(y,th,2)}$ , the red points show the time of the H to L-transition. The solid black curve represents the suggested operation boundary at which measures for handling the disruption should be started.

Based on such scenarios, initial experiments have been performed using the rise of the loop voltage,  $U_{loop}$ , the locked mode detector and the  $n = 1$  amplitude, as triggers. Any of these triggers initiates the application of ECCD at the  $q=2$  surface. In the

first experiments, the edge density rose above the cutoff density and the ECRH could not reach the resonant surface or was switched off immediately. An earlier trigger for initiating the ECCD was investigated. Based on the scaling of the HL-transition (equation (1)) an operational point at lower density, in the  $W_{mhd} - n_e(H-5)$  was chosen and the ECCD has been applied at a pre-programmed time. This was possible, as the gas puff rate was also pre-programmed and the discharges were highly reproducible. Disruptions were preventable with ECCD, reaching even further increased densities with constant high gas puff rate. A subsequent reduction of the gas puffing rate within the pre-programmed handler fully recovers the H-mode with high confinement, albeit at reduced density. This result could serve as a backup scenario at lower density (i.e. farther from the original higher density operational boundary). The left part of figure 3 shows a comparison between the naturally disrupting case and the case with the avoided disruption. This discharge had a plasma current of  $I_p = 0.6 MA$  and a toroidal field of  $B_t = -2.5 T$ . These values were chosen to make all flux surfaces accessible to the ECCD, and reduce the maximum  $n_e$  value of the density limit, assuming a Greenwald like dependence.

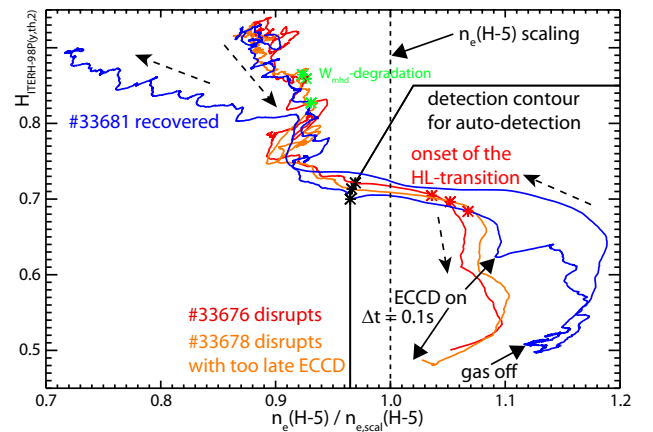


**Figure 5.** Operation diagram in terms of  $n_e(H-5)/n_{e,scal}(H-5)$  versus  $H_{ITERH-98P(y,th,2)}$  with trajectories from the disrupting reference discharge #33676, the saved and recovered discharge #33681 and the discharge #33678, where the ECCD has been applied too late and the discharge disrupts (see figure 3). In all cases the proposed trigger threshold would have been early enough to safely recover the discharge.

To combine the HL scaling and these experiments into a generic trigger that incorporates the H-mode density limit path,  $path_{HDL}$ , a further step is required. The global stored energy,  $W_{mhd}$ , must be replaced by the H-factor for H-mode scaling.  $ITER-98P(y,th,2)$  is the most appropriate scaling (equation (20) in [40]).

On the right hand side of figure 3 the trajectory of the disrupting case in the  $H_{ITER-98P(y,th,2)} - \bar{n}_e(H-5)/\bar{n}_{e,scal}(H-5)$  plane is shown. Clearly, the

loss of confinement at the HL-transition at roughly constant density can be seen. This time is the very last instant, at which a recovery with ECCD is feasible due to cutoff issues. Earlier in this discharge, at still lower density, a degradation of the confinement can be observed. This degradation is identified as an early time point to activate the corresponding HDL handler,  $handler_{HDL}$ , as the discharge can no longer be considered useful.

Using the database from [9], all H-mode density limit attempts with ECCD disruption avoidance were reinspected. For each discharge, the time of the HL-transition was noted (i.e. the sharp  $W_{mhd}$  drop at constant  $\bar{n}_e(H-5)$ ). Similarly, the time for a safe handler start was also noted. Figure 4 shows these data points in the  $H_{ITER-98P(y,th,2)} - \bar{n}_e(H-5)/\bar{n}_{e,scal}(H-5)$  plane. In this plane we define an empirical boundary identifying excessive density and insufficient L-mode confinement. Once the operation point (i.e. the state space description of the plasma) decreases towards the lower right corner ( $H_{ITER-98P(y,th,2)} \leq 0.85$  and  $\bar{n}_e(H-5)/\bar{n}_{e,scal}(H-5) \geq 0.965$  with a transition area), the handler for the H-mode density limit is activated. Figure 5 shows the trajectories of our reference case, the safely recovered case at high  $n_e$  and a case where the ECCD was applied too late. In the failed case, ECCD application terminated after 0.1s when it went into cutoff.

This operation boundary should still be considered as preliminary. Nevertheless, once a discharge transitioned to H-mode, no false alarms were observed. Discharges reaching the H-mode density limit have been correctly detected, and at a sufficient early enough time (i.e. before the post-shot identified time of the HL-transition). The histogram of the time difference  $\Delta t = t_{HL} - t_{auto}$  ( $t_{HL}$ : manually identified time of the H to L transition,  $t_{auto}$  automatically detected time for avoidance action) has a clear maximum around 0.1s and has no negative values. All these global parameters are reliably available in real-time, so that the state space point can be easily calculated. Only the density measurement from the interferometer can be unreliable when fringe jumps occur. The newly available density observer from RAPTOR can overcome this issue, as it combines measurements to correct for fringes jumps and can provide a density profile even in difficult conditions [18, 19].

## 5. Impurity induced disruption on TCV

Experiments for disruption avoidance at TCV have been performed successfully in H-modes which were generated by NBI and central ECRH heating. The toroidal field was selected so that the ECCD can

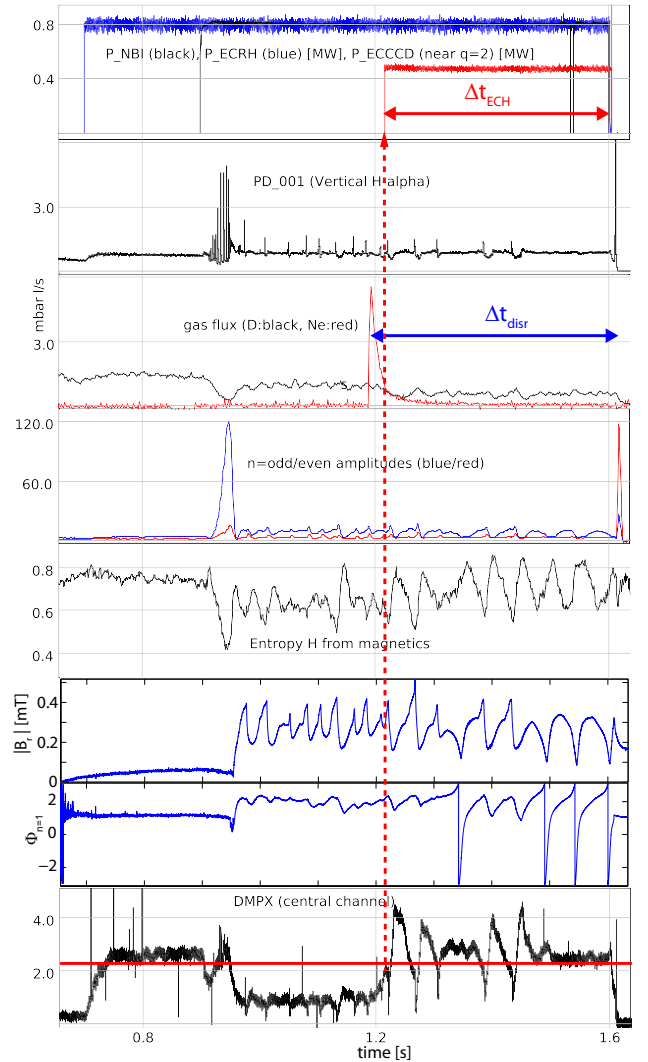


**Figure 6.** Time traces of a successfully recovered discharge. From top to bottom the time traces show: the applied central ECRH and NBI heating together with the triggered ECCD at the  $q=2$  surface, the  $H_\alpha$  emission in the divertor, the deuterium gas puff together with the neon puff, the  $n=1$  and  $n=2$  mode amplitudes, the entropy H from the SVD, the amplitude and the phase of the locked mode, and a central line of sight of the soft X-ray measurement. The duration of the ECCD pulse,  $\Delta t_{ECH}$ , and the time between the neon puff and the final disruption, after the ECCD has been switched off.

reach the  $q=2$  surface without cutoff issues. With the application of the NBI and the resulting LH-transition, a short phase of a rotating  $n=1$  mode occurs, which immediately locks. This is due to momentum balance between the externally applied NBI torque and the intrinsic plasma rotation torque. This degrades the H-mode confinement. A disruption was artificially caused by a pre-programmed neon puff to mimic the uncontrolled influx of impurities of abnormal events, i.e. mechanical failures in the vessel or failures in the control system. In figure 6, a successfully recovered case of such an injection is shown.

In these discharges the MHD activity begins so early at the LH-transition, that the usual MHD triggers, including the entropy trigger from the SVD could not be used as a trigger for ECCD. Instead, the increased radiated power due to the impurities was used as a trigger. This was measured by a sum of several core lines of sight of the soft X-ray array. A trigger was generated by an empirically defined threshold on this real-time signal.

A figure of merit for this approach is the applied ECCD pulse length,  $\Delta t_{EC}$ , before either safe discharge termination or final disruption occurs. Varying the ECCD deposition radius,  $\rho_{dep}^{ECCD}$ , showed that ECCD has to be localized around the  $q=2$  surface. This can be understood in terms of the  $n = 1$  locked mode that has a dominant  $m = 2$  component on this surface. The mode amplitude is reduced during the ECCD phase, and hence the mode is unlocking and can make several revolutions.

## 6. Summary and outlook

For ITER and DEMO, a new scheme for handling approaching disruptions has been developed and described. Recent experiments at ASDEX Upgrade and TCV were considered in such a framework. Experiments with H-mode density limits at ASDEX Upgrade with a new state-space based trigger and impurity puffed H-mode disruptions at TCV were presented. Central to success are the sensors and triggers tailored for the specific disruption path, rather than using generic, path independent sensors and triggers. The sensors have to be combined and used as a more general state space observers of the plasma rather than as individual measurements. In both cases, the ECCD actuator in the vicinity of the  $q=2$  surface was able to avoid an imminent disruption and recover towards stable discharge conditions.

## Acknowledgment

This work has been carried out within the framework of the EUROfusion Consortium and has received funding from the Euratom research and training programme 2014-2018 under grant agreement No 633053. The views and opinions expressed herein do not necessarily reflect those of the European Commission.

## References

[1] LEHNEN, M. et al., J. Nucl. Mater. **463** (2015) 39 .  
 [2] DE VRIES, P. C. et al., Nucl. Fusion **51** (2011) 053018.  
 [3] DE VRIES, P. C. et al., Plasma Phys. Controlled Fusion **21** (2014) 056101.  
 [4] PAUTASSO, G. et al., in *Europhysics Conference Abstracts (CD-ROM, Proc. of the 41th EPS Conference*

*on Plasma Physics, Berlin, Germany, 2014)*, volume 38F of *ECA*, page P2.015.  
 [5] KONOVALOV, S. et al., in *Proc. of the 26th IAEA Conference Fusion Energy (CD-Rom), Kyoto, Japan, October 2016*, volume 0, pages IAEA-CN-234/TH/7-1.  
 [6] MERTENS, V. et al., Plasma Physics and Controlled Fusion **36** (1994) 1307.  
 [7] MERTENS, V. et al., Nuclear Fusion **37** (1997) 1607.  
 [8] MERTENS, V. et al., Nuclear Fusion **40** (2000) 1839.  
 [9] BERNERT, M. et al., Plasma Physics and Controlled Fusion **57** (2015) 014038.  
 [10] NEU, R. et al., Journal of Nuclear Materials **438 Supplement** (2013) S34.  
 [11] NEU, R. et al., Plasma Science, IEEE Transactions on **42** (2014) 552.  
 [12] MARASCHEK, M. et al., in *Europhysics Conference Abstracts (CD-ROM, Proc. of the 40th EPS Conference on Plasma Physics, Espoo, Finland, 2013)*, volume 37D of *ECA*, page P4.127.  
 [13] CIANFARANI, C. et al., in *Europhysics Conference Abstracts (CD-ROM, Proc. of the 40th EPS Conference on Plasma Physics, Espoo, Finland, 2013)*, volume 37D of *ECA*, page P5.165.  
 [14] GALPERTI, C. et al., Plasma Phys. Controlled Fusion **56** (2014) 114012.  
 [15] REICH, M. et al., Fusion Science and Technology **61** (2012) 309.  
 [16] BERNERT, M. et al., Review of Scientific Instruments **85** (2014) 033503.  
 [17] MERTENS, V. et al., Fusion Science and Technology **44** (2003) 593.  
 [18] KUDLACEK, O. et al., in *Proc. of 44th EPS Conf. on Plasma Phys., Belfast, UK, 2017*, page P2.162.  
 [19] FELICI, F. et al., in *Proc. of 44th EPS Conf. on Plasma Phys., Belfast, UK, 2017*, page P1.151.  
 [20] STOBER, J. et al., Nuclear Fusion **43** (2003) 1265.  
 [21] ESPOSITO, B. et al., Nuclear Fusion **49** (2009) 065014.  
 [22] ESPOSITO, B. et al., Nuclear Fusion **51** (2011) 083051.  
 [23] MARASCHEK, M., in *Europhysics Conference Abstracts (CD-ROM, Proc. of the 42th EPS Conference on Plasma Physics, Lisbon, Portugal, 2015)*, volume 39E of *ECA*, page P1.112.  
 [24] REICH, M. et al., in *Europhysics Conference Abstracts (CD-ROM, Proc. of the 40th EPS Conference on Plasma Physics, Espoo, Finland, 2013)*, volume 37D of *ECA*, page P2.151.  
 [25] PETTY, C. C. et al., Nucl. Fusion **44** (2004) 243 .  
 [26] VOLPE, F. A. G. et al., Phys. Plasmas **16** (2009) 102502.  
 [27] VOLPE, F. A. et al., Phys. Rev. Lett. **115** (2015) 175002.  
 [28] PACCAGNELLA, R., in *Europhysics Conference Abstracts (CD-ROM, Proc. of the 43th EPS Conference on Plasma Physics, Leuven, Belgium, 2016)*, volume 40A of *ECA*, page P1.027.  
 [29] GRANUCCI, G., in *Europhysics Conference Abstracts (CD-ROM, Proc. of the 42th EPS Conference on Plasma Physics, Lisbon, Portugal, 2015)*, volume 39E of *ECA*, page P1.108.  
 [30] KULKARNI, S. et al., in *Proc. of the 25th IAEA Conference Fusion Energy (CD-Rom), St. Petersburg, Russian Federation, October 2014*, volume IAEA-CN-221, pages EX/P7-16.  
 [31] PAUTASSO, G., in *Europhysics Conference Abstracts (CD-ROM, Proc. of the 42th EPS Conference on Plasma Physics, Lisbon, Portugal, 2015)*, volume 39E of *ECA*, page P1.134.  
 [32] PAUTASSO, G. et al., Nuclear Fusion **47** (2007) 900.  
 [33] PAUTASSO, G. et al., Nuclear Fusion **36** (1996) 1291.  
 [34] PAUTASSO, G. and GRUBER, O., Fusion Science and Technology **44** (2003) 716.  
 [35] COMMAUX, N. et al., Nucl. Fusion **50** (2010) 112001.

- [36] RAPSON, C. J. et al., in *2016 41st International Conference on Infrared, Millimeter, and Terahertz waves (IRMMW-THz)*, pages 1–2, 2016.
- [37] RAPSON, C. J. et al., *Fusion Engineering and Design* **In press, corrected proof** (2017) .
- [38] RAPSON, C. et al., *Nuclear Fusion* **57** (2017) 076023.
- [39] KONG, M. et al., in *Proc. of 44th EPS Conf. on Plasma Phys., Belfast, UK, 2017*, page P4.152.
- [40] ITER Physics Expert Groups on Confinement and Transport and Confinement Modelling and Database, *Nucl. Fusion* **39** (1999) 2175 .